Title

Assessing Oximetry Response to Chimeric Antigen Receptor T-cell Therapy against Glioma with 19F MRI in a Murine Model

Journal

Radiology Imaging Cancer, 3(1)

ISSN

2638-616X

Authors

Chapelin, Fanny
Leach, Benjamin I
Chen, Ruifeng
et al.

Publication Date

2021

DOI

10.1148/rycan.2021200062

Peer reviewed

Radiology: Imaging Cancer

ORIGINAL RESEARCH

Assessing Oximetry Response to Chimeric Antigen Receptor T-cell Therapy against Glioma with ^{19}F MRI in a Murine Model

Fanny Chapelin, PhD • Benjamin I. Leach, PhD • Ruifeng Chen, MS • Deanne Lister, BS • Karen Messer, PhD • Hideho Okada, MD, PhD • Eric T. Ahrens, PhD

From the Department of Biomedical Engineering, University of Kentucky, Lexington, Ky (F.C.); Department of Radiology (B.I.L., D.L., E.T.A.), Department of Biostatistics and Bioinformatics (R.C.), and Department of Family Medicine and Public Health (K.M.), University of California San Diego, 9500 Gilman Dr, La Jolla, CA 92093; Department of Neurologic Surgery, University of California San Francisco, San Francisco, Calif (H.O.); and Parker Institute for Cancer Immunotherapy, San Francisco, Calif (H.O.). Received May 19, 2020; revision requested July 17; revision received August 10; accepted September 24. **Address correspondence to** E.T.A. (e-mail: *eta@ucsd.edu*).

Supported by the National Institutes of Health (grants R01-EB017271, R01-EB024015, and R01-CA139579) and California Institute for Regenerative Medicine (grant LA1-C12-06919).

Conflicts of interest are listed at the end of this article.

See also commentary by Bulte in this issue.

Radiology: Imaging Cancer 2021; 3(1):e200062 • https://doi.org/10.1148/rycan.2021200062 • Content codes: NR OI

Purpose: To assess the cell-specific, intracellular partial pressure of oxygen (Po_2) dynamics of both tumor and chimeric antigen receptor (CAR) T cells in a murine immunotherapy model.

Materials and Methods: Human glioblastoma cells or human T cells were intracellularly labeled with perfluorocarbon nanoemulsion droplet sensors prior to in vivo injection in severe combined immunodeficient mice to measure Po_2 in the two cell types in response to treatment. Two main sets of experiments were performed: *(a)* mice were injected in the flank with perfluorocarbon-labeled human glioblastoma cells and were then inoculated with either CAR T cells or untransduced T cells or were untreated 5 days after tumor inoculation; and *(b)* mice with unlabeled glioblastoma tumors were inoculated with perfluorocarbon-labeled CAR T cells or untransduced T cells 5 days after tumor inoculation. Longitudinal fluorine 19 (^{19}F) spin-lattice relaxation time measurements of the tumor mass were used to ascertain absolute Po_2 in vivo. Results were analyzed for significance using an analysis of variance, a linear mixed-effect model, and a Pearson correlation coefficient test, as appropriate.

Results: The intracellular tumor cell Po_2 temporal dynamics exhibited delayed, transient hyperoxia at 3 days after infusion of CAR T cells, commensurate with significant tumor cell killing and CAR T-cell infiltration, as observed by bioluminescence imaging and histologic findings. Conversely, no significant changes were detected in CAR or untransduced T-cell intracellular Po_2 over time in tumor using these same methods. Moreover, it was observed that the total ^{19}F tumor cell signal quenches with treatment, consistent with rapid tissue clearance of probe from apoptotic tumor cells.

Conclusion: Cell-specific Po_2 measurements using perfluorocarbon probes can provide insights into effector cell function and tumor response in cellular immunotherapeutic cancer models.

Supplemental material is available for this article.

Recent cancer therapy efforts have focused on efficient and targeted tumor cell killing and hypoxia reduction (1,2). Adoptive cell therapy has emerged as the fourth pillar of cancer therapy, offering specific eradication of hematologic cancers. Therapeutic cell engineering is now being used to target solid tumors, which are proving to be more challenging (3,4). Roadblocks include tumor-induced immunosuppression and inefficient cell trafficking as well as poor tumor penetration and persistence (4,5). Importantly, these characteristics may be predictive of therapeutic outcome. Tumor mechanisms of immunosuppression generate chronic inflammation and hypoxia in the vicinity of the tumor, which result in increased tumor angiogenesis, recurrence, and malignant progression (1,6). Effector cells in the tumor microenvironment can induce cell killing, and we hypothesize that tumor oximetry is altered as an indirect consequence of these apoptotic processes.

Recent advances in noninvasive imaging and biosensor probe technologies enable the noninvasive, real-time observation of the intracellular partial pressure of oxygen (Po_2) during T cell–mediated immunotherapy. Moreover, perfluorocarbon (PFC) exhibits weak molecular cohesion, enabling gas dissolution (7). This intrinsic property was first exploited in the 1990s (8) using emulsified PFC to form biocompatible and injectable oxygen-laden blood substitutes and breathing liquids (9,10). Gas dissolved in fluorinated emulsions is not bound to the carrier but rather is exchanged with the local environment (11). Dissolution of oxygen in PFC lowers the fluorine 19 (^{19}F) spin-lattice relaxation time (T1) (10,12). The T1 varies linearly with the absolute Po_2, which is calculated from a linear calibration curve (13–16). Thus, one can exploit the intracellular PFC label, with its intrinsic Po_2 sensing properties, to perform cell-specific oximetry in vivo (15,16).

Abbreviations

BLI = bioluminescence imaging, CAR = chimeric antigen receptor, PBS = phosphate-buffered saline, PFC = perfluorocarbon, Po_2 = partial pressure of oxygen, RARE = rapid acquisition with relaxation enhancement, R1 = relaxation rate, TAT = transactivating transcription sequence, TE = echo time, TR = repetition time, TUNEL = terminal deoxynucleotidyl transferase–mediated dUTP nick end labeling, T1 = spin-lattice relaxation time, U87-EGFRvIII-Luc = cell line overexpressing epidermal growth factor receptor variant III and the luciferase gene

Summary

Fluorine 19 (^{19}F) MRI enables temporal measurements of tumor cell oxygen tension in response to chimeric antigen receptor T-cell therapy; these data support the view that ^{19}F partial pressure of oxygen MRI can provide insights into the modes of action of engineered T-cell immunotherapy against cancer.

Key Points

- Longitudinal tumor cell oximetry displays a delayed, transient hyperoxia upon infusion of chimeric antigen receptor T-cell therapy, thus providing insights into effector cell function in vivo.
- In contrast to tumor cell oximetry, oximetry changes in fluorine-labeled T cells were not resolved using these methods.
- The fluorine 19 (^{19}F) MRI signal loss of labeled tumor cells upon T-cell treatment correlated to tumor killing, as observed by bioluminescence imaging, suggests effective tissue clearance of ^{19}F probe in apoptotic cells.

Our approach uses PFC nanoemulsion imaging tracer probes, used in conjunction with ^{19}F MRI, for background-free cell detection (16,17). Ex vivo labeling of cells with PFC nanoemulsion can be performed by addition to the culture media. The PFC nanoemulsion is only taken up by viable cells, which retain the tag without cell efflux. Following delivery of the labeled cells to the patient, ^{19}F MRI enables quantitative cell detection (ie, in vivo cytometry), a method that has been demonstrated clinically (18). Upon death of the labeled cells, PFC droplets disperse and the ^{19}F signal dissipates. Rose et al (19) suggested that fluorine retention can be used as a surrogate marker for cell survival.

In this study, we test the hypothesis that a measurable change in tumor and/or T-cell Po_2 is commensurate with chimeric antigen receptor (CAR) T-cell apoptotic processes in a xenograft murine model of subcutaneous glioblastoma targeted with human CAR T cells. Overall, we found that monitoring of tumor and T-cell Po_2 provides an in vivo marker for monitoring cellular immunotherapeutics, and potentially for optimizing therapeutic course, dosage, and elucidation of mechanisms of action.

Materials and Methods

PFC Nanoemulsion Formulations

Aqueous nanoemulsion was gravimetrically prepared from the PFC perfluoro-15-crown-5 ether (Exfluor Research, Round Rock, Tex) and 5% by weight Pluronic F68 (Spectrum Chemical, Gardena, Calif) surfactant as previously described (20). Specific details of synthesis can be found in Appendix E1 (supplement).

An alternative PFC nanoemulsion formulation displayed a cell-penetrating peptide as a component of the surfactant to boost cell labeling in T cells and other weakly phagocytic cell types (21), namely, the transactivating transcription sequence (TAT) of the human immunodeficiency virus. Details on the synthesis of the TAT conjugate are found in Appendix E2 (supplement).

Nanoemulsion concentrations and Po_2 calibration curve were determined by nuclear magnetic resonance. Details are described in Appendix E3 (supplement).

Human T Cells and CAR Transduction

Using anonymous donor human blood (San Diego Blood Bank, San Diego, Calif), primary human T cells were enriched by Ficoll (Histopaque-1077; Sigma Aldrich, St Louis, Mo) gradient density centrifugation and pan-T magnetic cell sorting (MACS; Miltenyi Biotech, Auburn, Calif). Protocol for CAR transduction of human T cells is found in Appendix E4 (supplement).

Glioblastoma Cells

A human glioblastoma multiform cell line (23) overexpressing the epidermal growth factor receptor variant III and the luciferase gene (U87-EGFRvIII-Luc) was maintained in T75 flasks (Sigma) in Roswell Park Memorial Institute medium, supplemented with 10% fetal bovine serum.

Ex Vivo Cell Labeling

For glioma labeling experiments, U87-EGFRvIII-Luc were plated at 90% confluence (triplicates of 1×10^6 cells in 2 mL media per well) and incubated overnight with different PFC nanoemulsion concentrations ranging from 2.5 to 20 mg/mL. For in vivo experiments, an optimal concentration of 20 mg/mL PFC was added overnight to U87-EGFRvIII-Luc cells. Cells were counted and rinsed three times in phosphate-buffered saline (PBS), and 5×10^6 cells were resuspended in buffered 50% Corning Matrigel (Corning Life Sciences, Tewksbury, Mass) for a 100-μL flank injection volume.

For intratumoral injections, CAR and untransduced T cells were labeled overnight with 15 mg/mL TAT-PFC nanoemulsion with 10^7 cells per well in 5 mL of media using six-well plates. Cell viability after labeling was confirmed by the trypan blue exclusion assay. The cells were washed in 0.05% trypsin for 3 minutes to remove possible extracellular label, de-beaded on a magnet, and rinsed twice in PBS. Cells were resuspended in PBS at a concentration of 10^7 cells per 50 μL for intratumoral injection. Measurement of PFC uptake after labeling is described in Appendix E3 (supplement).

Murine Model of Subcutaneous Glioblastoma

Animal protocols were approved by the University of California San Diego Institutional Animal Care and Use Committee. In the first cohort, female (n = 18) 6–8-week-old severe combined immunodeficient mice (Jackson Laboratories, Bar Harbor, Maine) received subcutaneous unilateral flank tumor injections composed of 5×10^6 PFC-labeled glioma cells. Five

days after tumor inoculation (day 0 time point), mice were divided into three groups. Group 1 (n = 6) mice received 2×10^7 CAR T cells injected intravenously in PBS. Group 2 (n = 6) mice received the same number of untransduced T cells intravenously. A second control group (group 3) remained untreated (n = 6).

In the second cohort, the same strain of mice (n = 12) received subcutaneous unilateral flank injections of 5×10^6 unlabeled glioma cells. Five days after tumor inoculation (day 0 time point), mice were divided into two groups. Group 4 (n = 6) received 1×10^7 TAT-PFC–labeled CAR T cells in PBS injected intratumorally, and group 5 (n = 6) received the same number of TAT-PFC–labeled untransduced T cells intratumorally.

In Vivo Bioluminescence Imaging

Longitudinal bioluminescence imaging (BLI) was performed on day 0, 1, 3, 7, and 10 using an IVIS Spectrum system (PerkinElmer, Waltham, Mass). D-luciferin (Intrace Medical, Lausanne, Switzerland) was administered intraperitoneally at a dose of 150 mg/kg 10 minutes prior to imaging. Mice were anesthetized (2% isoflurane in oxygen) during BLI. Regions of interest were defined as a circle encompassing the luminescent signal from each tumor, and the total flux (photons/sec) was calculated using Living Image Software (PerkinElmer). Following BLI, tumor sizes were measured using a caliper.

MRI Scans

MRI was performed on the same days as BLI. For groups 4 and 5, day 0 corresponds to imaging 2 hours after intratumoral injection of T cells. MRI details can be found in Appendix E5 (supplement). MRI measurements were performed with an 11.7-T Bruker BioSpec preclinical scanner (Bruker, Billerica, Mass) with a dual-tuned ^{1}H/^{19}F birdcage volume coil (Bruker).

The ^{19}F images were acquired using a rapid acquisition with relaxation enhancement (RARE) sequence with the following parameters: repetition time (TR), 2000 msec; echo time (TE), 13 msec; RARE factor, four; matrix, 64×46; field of view, 32×24 mm^2; spatial resolution, 0.5×0.5 mm^2; section thickness, 1 mm; 32 averages; and 12 sections. ^{1}H anatomic images were also acquired using the RARE sequence, with TR, 2000 msec; TE, 14 msec; RARE factor, two; matrix, 256×184; field of view, 32×24 mm^2; spatial resolution, 0.125×0.13 mm^2; section thickness, 1 mm; two averages; and 12 sections. The total tumor ^{19}F signal (ie, total fluorine atoms) at each time point was calculated from raw image data using Voxel Tracker software (Celsense, Pittsburgh, Pa), which incorporates the external reference and image noise as described elsewhere (24,25).

The ^{19}F T1 values were measured using a point-resolved spectroscopy sequence, by defining a voxel encompassing the entire tumor mass (approximately $8 \times 8 \times 8$ mm^3). Twelve TR values were used, ranging between 0.1 and 6 seconds, with a total acquisition time of approximately 30 minutes. Imaging bandwidth was adjusted to exclude potential interference of the isoflurane signals on spectra, as described elsewhere (26). The T1 values were fit using a three-parameter single exponential equation in MNova software (version 6.0.2; Mestrelab Research, Santiago de Compostela, Spain). The mean Po_2 of the tumor cells and CAR T cells was calculated from T1 using a calibration curve (15,16).

Histologic Examination

Additional animals identical to groups 1 and 2, referred to as groups 6 and 7, were prepared (n = 3, per group) for apoptotic and T-cell counts in tumors. Details on histologic sample preparation and staining for CD3 and apoptotic cells are found in Appendix E6 (supplement).

Statistical Analysis

All measurements are presented as mean ± standard error. Results were analyzed for significance using an analysis of variance, a linear mixed-effect model, and a Pearson correlation coefficient test, as appropriate. More details can be found in Appendix E7 (supplement).

Results

Longitudinal ^{19}F MRI and Glioma Burden

To label glioma cells, PFC nanoemulsion was formulated with a mean droplet size of 176 nm ± 4 (standard deviation) and polydispersity index of 0.10 ± 0.02 as measured by dynamic light scattering. Prior to implantation, U87-EGFRvIII-Luc cells were labeled overnight ex vivo with PFC to an average level of approximately 7×10^{12} ^{19}F atoms per cell, as measured with ^{19}F nuclear magnetic resonance (Fig E1 [supplement]). Five days after flank tumor implantation, baseline imaging (day 0) was performed prior to cell therapy infusion. Anatomic ^{1}H axial images show the presence of a solid tumor in the right flank of mice (Fig 1, *A*, left). The ^{19}F image reveals a bright hotspot in the tumor in the displayed field of view (Fig 1, *A*, right). The ^{19}F signal was detected in one to three contiguous tumor sections, where only a single section is displayed (Fig 1, *A*, right). Maximum pixel signal-to-noise ratio at day 0 was approximately 51. The longitudinal composite ^{1}H/^{19}F images (day 0, 7, and 10) show clearance of PFC signal over time in CAR T-cell–treated tumors (Fig 1, *B*). In untransduced T-cell–treated tumors, PFC hotspot remains stable at day 10 (Fig 1, *C*). We note that postprocessing thresholding of the pseudocolor images (Fig 1) masks low-level ^{19}F signal in image display.

Longitudinal bioluminescence measurements show significant tumor burden reduction 7 days after CAR T-cell treatment with an average radiance of 4×10^{10} photons/sec, which is half of the radiance measured for both naive T-cell–treated and –untreated groups (F[2,12] = 7.585; P = .007) (Fig 2, *A*). The ^{19}F content in the two control groups did not change significantly over 10 days (P = .1 and P = .2, respectively), whereas the CAR T-cell–treated tumors exhibited significant ^{19}F reduction (approximately 60% signal loss; P = .001) (Fig 2, *B*). Signal loss between groups was significant as early as day 3 (P = .03) (Fig 2, *B*). There was a strong negative correlation between absolute tumor ^{19}F content and BLI radiance in all groups (Pearson $r = -0.85 < r < -0.98$) (Fig 2, *C*). The PFC droplets are neither broken down, nor do they

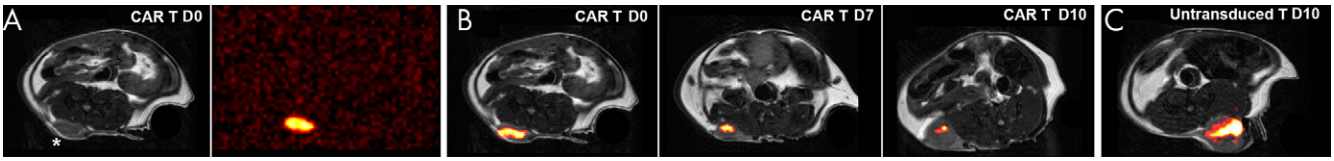

Figure 1: In vivo fluorine 19 (^{19}F) signal in glioma tumor after intravenous chimeric antigen receptor T-cell (CAR T) therapy. *A*, Proton (^{1}H) axial MRI of mouse abdomen (left) with flank tumor (*) and ^{19}F image (right) with perfluorocarbon-labeled glioma cells appearing as a bright hotspot. *B*, Composite ^{1}H/^{19}F images of a mouse receiving CAR T cells at day 0 (D0, left), 7 (D7, middle), and 10 (D10, right). Representative longitudinal overlays of a CAR T-cell–treated mouse show modest tumor growth and decreased ^{19}F signal as a result of cytotoxic T-cell therapy. *C*, In comparison, mice receiving untransduced T cells exhibit persistent fluorine signal at day 10 (D10). Here, ^{19}F signal is detected in one to three contiguous tumor sections, where only a single section is displayed at each time point.

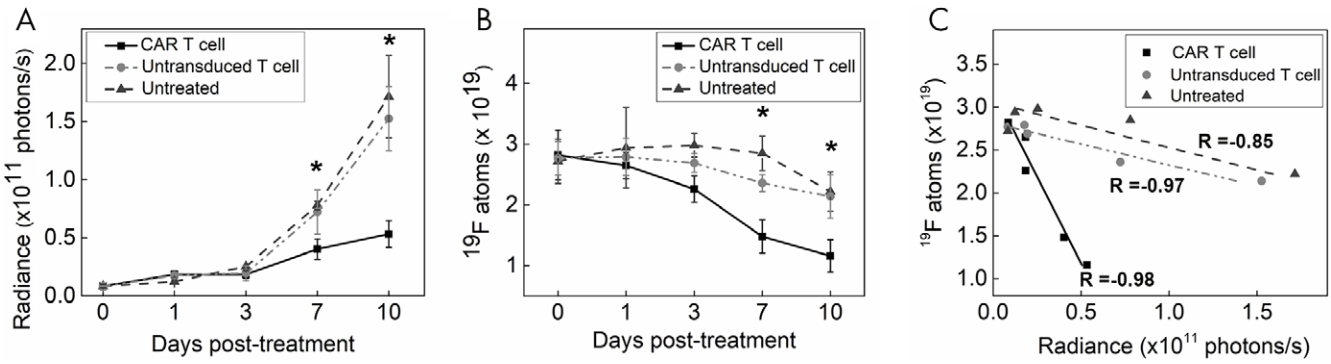

Figure 2: Effect of intravenously delivered chimeric antigen receptor (CAR) T cells on tumor growth and total fluorine content. *A*, Longitudinal bioluminescence measurements show half as much radiance in CAR T-cell–treated animals compared with controls at day 7 (*P = .01). By day 10 the radiance gap widens, representing significant tumor growth reduction in the CAR T-cell–treated group (*P = .01). Data are presented as mean ± standard error. *B*, Total fluorine 19 (^{19}F) content in the tumors as measured by longitudinal MRI. Here, the total ^{19}F content is measured in all contiguous sections in tumor region that shows detectable signals. Control groups do not exhibit significant ^{19}F signal loss over 10 days, whereas in CAR T-cell–treated animals ^{19}F signal decreases by approximately 60% in the same period. Data are presented as mean ± standard deviation (*P = .01). *C*, Comparison of total fluorine atoms to bioluminescence signal in tumors yields a strong negative correlation (Pearson $r = -0.85 < r < -0.98$) in all groups (n = 25 per group), suggesting that total fluorine signal is an indicator of tumor killing and putative therapeutic efficacy.

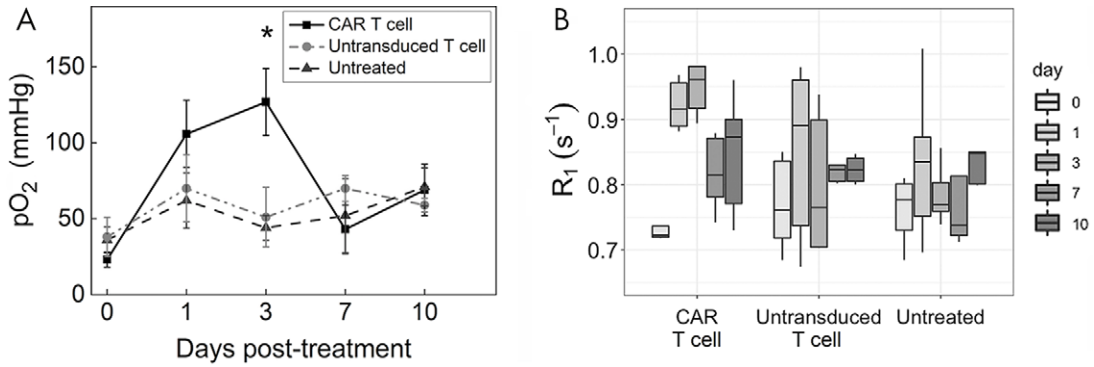

Figure 3: Longitudinal glioma tumor partial pressure of oxygen (Po_2) after chimeric antigen receptor (CAR) T-cell therapy. *A*, Summary of tumor cell Po_2 results following systemic delivery of CAR T cells or untransduced T cells as well as results of untreated controls. A significant increase in tumor Po_2 in CAR T-cell–treated animals was observed at day 3 after infusion (*P = .0114). The Po_2 is calculated from the fluorine 19 (^{19}F) relaxation rates (R1), measured from magnetization recoveries of the recorded ^{19}F signal. Data are presented as mean ± standard error. *B*, Box plots of R1 data for each experimental group on day 0, 1, 3, 7, and 10.

undergo exocytosis by the cell (27). Signal loss is presumably attributed to glioma cell death as well as scavenging and removal of cell contents by itinerant macrophages, as described elsewhere (22). Thus, the ^{19}F signal is inversely proportional to tumor burden and therefore may function as a therapeutic marker in preclinical models.

In Vivo Glioma Oximetry

Localized ^{19}F MR spectroscopy, with a single voxel encompassing the tumor, was used to measure relaxation rate (R1) values. Absolute tumor Po_2 was calculated from the measured R1 using a calibration curve (Fig E2 [supplement]). A summary of the longitudinal tumor cell Po_2 results is shown in

Figure 3, *A*. Notably, a transient spike was observed in tumor Po_2 3 days after CAR T-cell infusion (R1 = 0.99 sec^{-1} ± 0.12; Po_2 = 134 mm Hg ± 25) (Fig 3), which was not observed for untransduced T cells (Po_2 = 61 mm Hg ± 20) or controls (Po_2 = 40 mm Hg ± 9, $F[2,12] = 6.653$; $P = .0114$ for analysis of variance of all day 3 groups) (Table E1 [supplement]). There was no significant Po_2 change in the control groups at day 3 (*t* test; $P = .35$). By day 7, tumor oxygenation returned to baseline in the CAR T cell (Fig 3, *A*). These data suggest specific CAR T-cell homing to the tumor tissue, presumably initiating a target killing cascade that transiently alters intracellular Po_2.

In further analysis, the R1 values for groups 1–3 are displayed as box plots in Figure 3, *B*. The linear mixed-effects statistical model demonstrates a significant difference in R1 between CAR T-cell–treated and untransduced T-cell–treated mice (treatment effect, 0.23; adjusted 95% CI: 0.01, 0.45) and untreated mice (treatment effect, 0.26; adjusted 95% CI: 0.05, 0.47) (Table E1 [supplement]) on day 3 with respect to day 0 that returns to baseline by day 7.

In Vivo MRI and MR Spectroscopy of T-cell Po_2

To monitor effector cell oximetry in vivo, we labeled CAR T cells prior to intratumoral delivery to the flank glioma model. T cells labeled overnight with TAT-PFC nanoemulsion show no significant viability impairment (Fig E3A, E3B [supplement]). Additionally, phenotypic studies show no changes in CD4 and CD8 expression following TAT-PFC labeling (Figure E3C, E3D [supplement]). Longitudinal MRI $^1H/^{19}F$ overlay images of labeled CAR T cells and untransduced T cells are displayed in Figure 4. For mice receiving CAR or untransduced T cells (groups 4 and 5, respectively), day 0 corresponds to imaging 2 hours after T-cell injection. The inoculated cells remained in the tumor vicinity during the 10-day imaging period (Figs 4, 5, *D*). CAR T cells and untransduced T cells do not show significant changes in Po_2 upon contact with tumor cells (Fig 5, *A, B*). The longitudinal Po_2 measurements for these groups are displayed in Figure 5, *A*, and R1 values are displayed as box plots in Figure 5, *B*. The linear mixed-effects model shows no statistical significance between CAR T cells and untransduced T cells at either time point with respect to day 0 (treatment effect day 1, −0.17 [adjusted 95% CI: −0.42, 0.08]; day 3, −0.06 [95% CI: −0.32, 0.19]; day 7, −0.10 [95% CI: −0.36, 0.16]; day 10, 0.09 [95% CI: −0.17, 0.35]). When injected, CAR T cells remained cytotoxic toward cancer cells compared with untransduced T cells, as evidenced by lower tumor BLI signal as early as day 7 ($P = .001$) (Fig 5, *C*). Absolute fluorine content of locally injected T cells in groups 4 and 5 did not change over 10 days ($P = .79$ and $P = .26$, respectively) (Fig 5, *D*), in contrast to labeled glioma cells (Fig 2, *B*). Importantly, persistence of intracellular fluorine label in viable T cells has previously been established in vitro and in vivo in the same CAR T-cell–glioma treatment model used in this study using a fluorescent PFC emulsion and subsequent colocalization of the fluorescent signal in T cells by histopathology (22).

Histologic Assessment of the Tumor Environment after T-cell Treatment

Histologic analyses confirm intracellular localization of PFC in glioma cells and the presence of T cells in tumors (Fig E4 [supplement]). Green fluorescent protein–expressing U87 cells labeled with fluorescently conjugated PFC nanoemulsion (28) prior to implantation display intracellular localization of PFC droplets and green fluorescent protein (group 8), thus supporting the origins of the measured Po_2 values. Overall, viable cells retain PFC label in lysosomal vesicles long term, as detailed elsewhere (27).

Immunohistochemical staining of tumors at day 3 after cell transfer confirms the presence of numerous CAR T cells in the tumor (group 6) and, to a lesser extent, untransduced T cells (group 7), as shown in Figure 6, *A*. Terminal deoxynucleotidyl transferase–mediated dUTP nick end labeling staining revealed numerous apoptotic cells in the vicinity of CAR T cells, whereas few to no apoptotic cells were seen in untransduced T-cell–treated tumors (Fig 6, *A*). In groups 6 and 7, more than twice the number of CAR T cells infiltrated the tumor compared with untransduced T cells ($P < .001$) (Fig 6, *B*). CAR T-cell–treated tumor slices display numerous apoptotic tumor cells, whereas few apoptotic cells were found in untransduced T-cell–treated tumors ($P < .001$) (Fig 6, *C*). The number of CAR T cells present correlated with the number of apoptotic cells per field (Pearson $r = 0.67$) whereas untransduced T cells did not (Pearson $r = -0.31$) (Fig 6, *D*). These observations are consistent with CAR T cells exhibiting specific cytotoxic activity toward glioma cells in vivo. Untransduced T cells, despite reaching the tumor site, did not induce significant cell apoptosis.

Discussion

We investigated the use of PFC probe biosensors and ^{19}F MRI for real-time monitoring of the intracellular Po_2 response to CAR T-cell therapy against glioma. Peak glioma Po_2 was observed 3 days after infusion and suggests significant CAR T-cell infiltration and targeted tumor cell killing, compared with untransduced T cells. Loss of glioma cell fluorine signal in the tumor correlated to reduction in tumor bioluminescence signal, suggesting effective tissue clearance of probe from apoptotic cells. In addition, CAR T-cell numbers in the tumor at day 3 correlated to cancer cell apoptosis, whereas untransduced T cells did not generate significant apoptosis. CAR T-cell and untransduced T-cell Po_2 did not change significantly upon contact with tumor cells; nonetheless, the inoculated cells remained in the tumor vicinity during the imaging period (10 days). The observation of a transient increase in Po_2 in glioma target with therapeutic T-cell infusion can be viewed as a real-time assay of anticancer effect and can potentially be used to evaluate cell therapy candidates preclinically, as well as to predict the optimal timing for redosing to maximize therapeutic efficacy. Moreover, Po_2 increase in the CAR T-cell–treated group was short-lived, suggesting insufficient therapeutic cell homing to the tumor and possible CAR T-cell exhaustion or tumor immunosuppression (29), each being a key bottleneck in adoptive cell therapy.

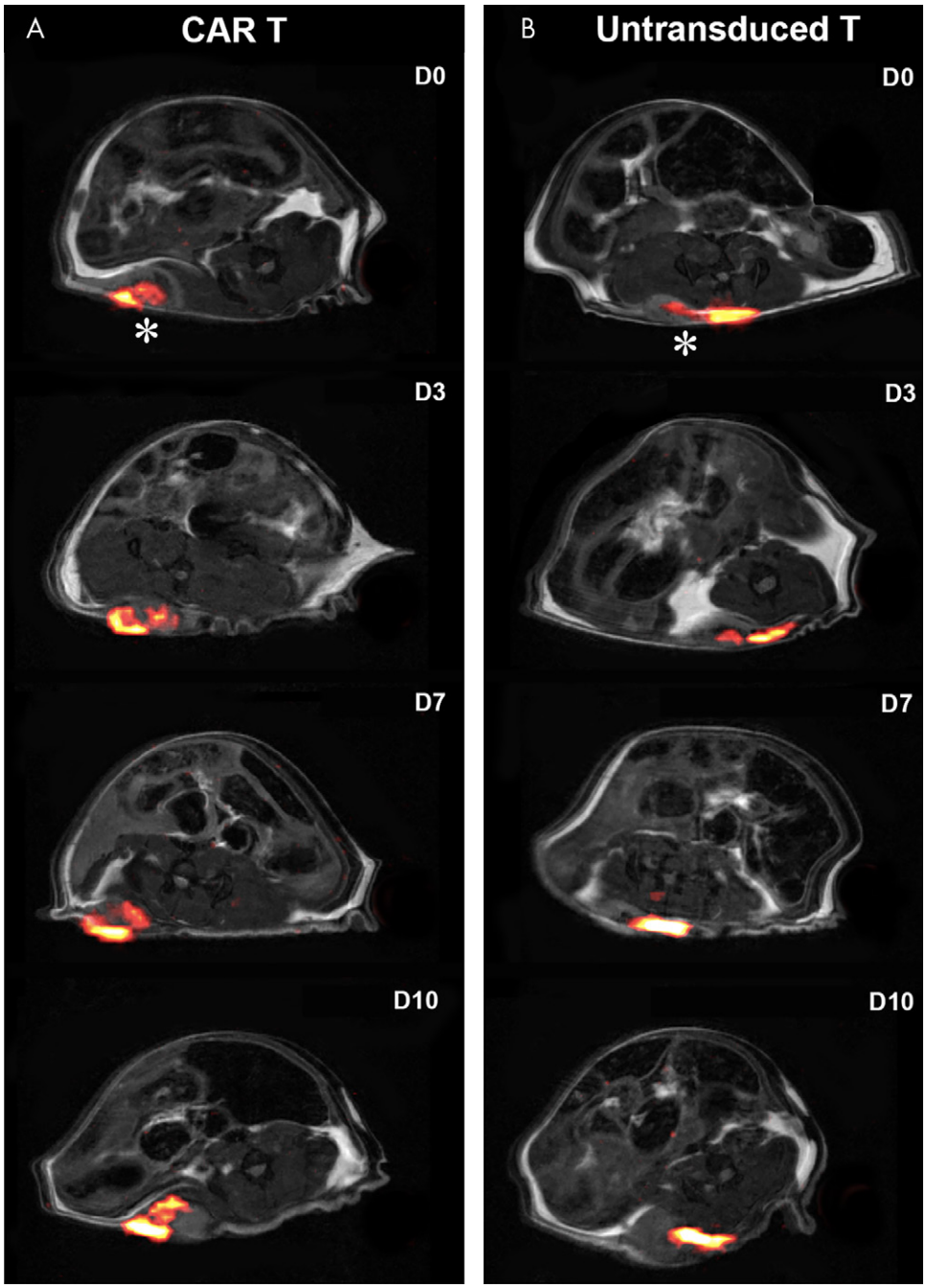

Figure 4: Longitudinal in vivo imaging of perfluorocarbon-labeled chimeric antigen receptor (CAR) T cells delivered intratumorally. Shown are time-series proton and fluorine 19 images of the mouse abdomen bearing a flank tumor (*) with, *A*, perfluorocarbon-labeled CAR T cells (CAR T) or, *B*, untransduced T cells (untransduced T) at day (D) 0, 3, 7, and 10 after intratumoral injection. The data demonstrate accurate intratumoral delivery of T cells (hotspots) and persistent signal consistent with T-cell survival.

Neither CAR T cells nor control T cells exhibited significant Po_2 changes over the course of 10 days by these techniques in this model. Generally, T cells undergo metabolic activation (30) upon binding to their specific antigen, resulting in increased oxygen consumption rate with the initiation of the killing cascade (31). We speculate that CAR T cells may tightly regulate their intracellular oxygen content, resulting in no apparent Po_2 change despite increased oxygen consumption rate. In addition, CAR T cells in the tumor are likely to be heterogeneous metabolically, with some cells clearly displaying effector functions, as evidenced by active tumor cell killing, and some T cells being exhausted or of CD4+ phenotype. Nonetheless, CAR T cells injected intratumorally generated significant tumor growth reduction compared with their untransduced T-cell counterparts. As expected from the high number of cells delivered to the tumor, intratumoral injection of CAR T cells showed evident advantage over systemic injection based on BLI measurements (P = .04 at day 10). CAR T cells were not injected systemically

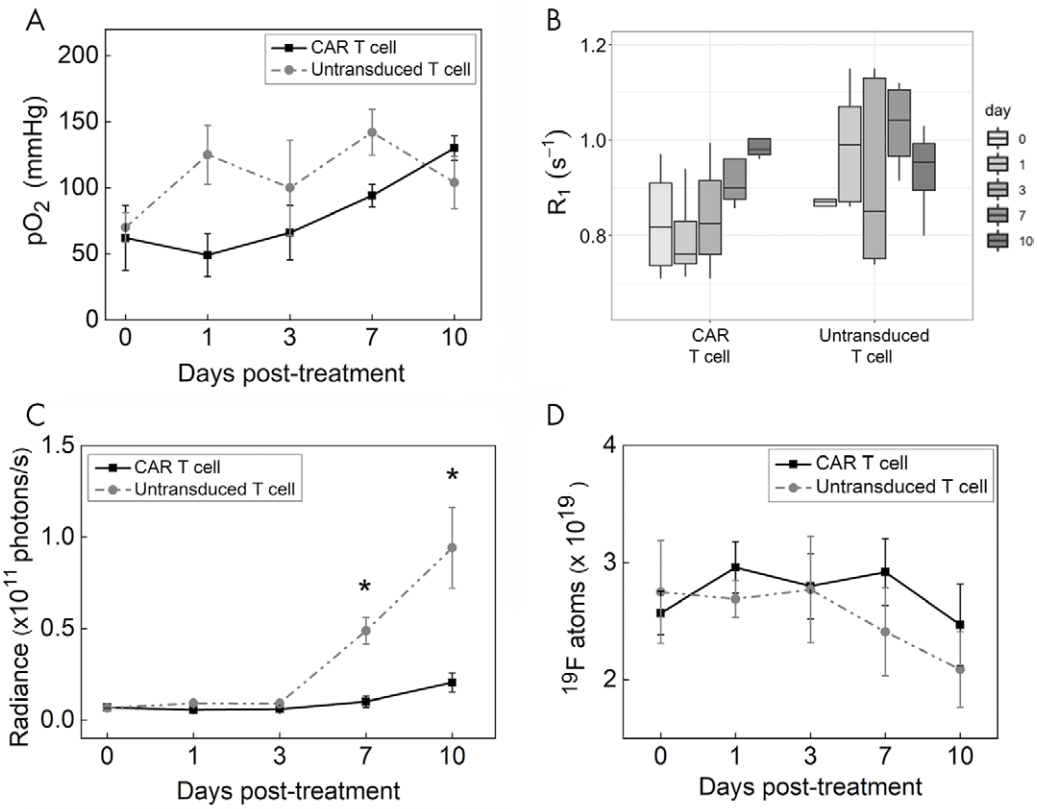

Figure 5: In vivo chimeric antigen receptor (CAR) T-cell partial pressure of oxygen (Po_2) in tumor microenvironment. *A*, Summary of longitudinal T-cell Po_2 measurements for intratumoral perfluorocarbon-labeled CAR T cells and untransduced T cells. *B*, Corresponding relaxation rate (R1) data as box plots are shown. CAR T-cell and untransduced T-cell Po_2 did not vary significantly over a 10-day monitoring period. *C*, Bioluminescence measurements show significantly lower radiance in CAR T-cell–treated animals compared with controls at day 7 (*$P < .001$), indicating a therapeutic effect. By day 10, the radiance gap widens, representing significant tumor growth reduction in the CAR T-cell–treated group (*$P = .009$). *D*, Absolute fluorine content of locally injected CAR T cells and control cells, by ^{19}F MR spectroscopy, did not change significantly over 10 days ($P = .79$ and $P = .26$, respectively), suggesting labeled T-cell persistence.

in the present study because homing efficiency to tumor is low in this model (19) and does not result in sufficient signal to yield reliable T1 measurements.

PFC labeling of tumor or T cells prior to injection enables uniform label distribution and circumvents biases resulting from local or systemic injection of tracer agent. Labeled cells retain the PFC label in situ, and mitosis results in symmetric partitioning of the PFC label to daughter cells (27). Po_2 sensing by ^{19}F MR spectroscopy is independent of the concentration of PFC in the cell (16); thus, cell division and probe dilution is not predicted to affect R1 measurement. Labeled cell death results in PFC dispersion and uptake predominately to Kupffer cells of the liver, as discussed elsewhere (22).

Although the mechanism of oxygen regulation in cancer cells after treatment is understudied, we speculate that the perforins released by CAR T cells upon binding to their cancer target is responsible for increased oxygen tension in the apoptotic cancer cell (32). The apoptotic pathway initiated by CAR T cells is expected to lead to tumor cell mitochondrial membrane permeabilization and reduced oxidative phosphorylation (33,34) and, potentially, reduced oxygen consumption. The Po_2 measurements presented here build on prior results using ^{19}F MR oximetry to monitor response to chemotherapy (15) and cytotoxic T cells (16). With similar methods used here, Kadayakkara et al (15) reported basal Po_2 of approximately 45 mm Hg in rat glioma cells, and treatment with a chemotherapeutic agent resulted in a sustained Po_2 increase to approximately 165 mm Hg over 72 hours. Zhong et al (16) used a murine model of glioma treated with Pmel-1 cytotoxic T cells and showed a transient Po_2 increase (approximately 94 mm Hg) 2 days after infusion. In earlier studies, PFC nanoemulsion was directly injected intravenously, thereby enabling vasculature imaging (35–37) and tissue oximetry measurements in vivo (38–41).

Established methods for in vivo oxygenation measurements, such as electrodes or fiber-optic sensors (42,43), require invasive insertion of probes in tumors, resulting in tissue and vascular damage, inflammation, and probe sampling bias. Blood oxygen level changes can be indirectly observed by monitoring relative levels of diamagnetic oxyhemoglobin and paramagnetic deoxyhemoglobin via conventional ^{1}H MRI (44). Hemoglobin, devoid of oxygen, shortens the relaxation times of surrounding water protons, particularly T2, giving rise to blood oxygen level–dependent MRI contrast. Blood oxygen level–dependent MRI signal changes reflect vasculature and nearby parenchyma

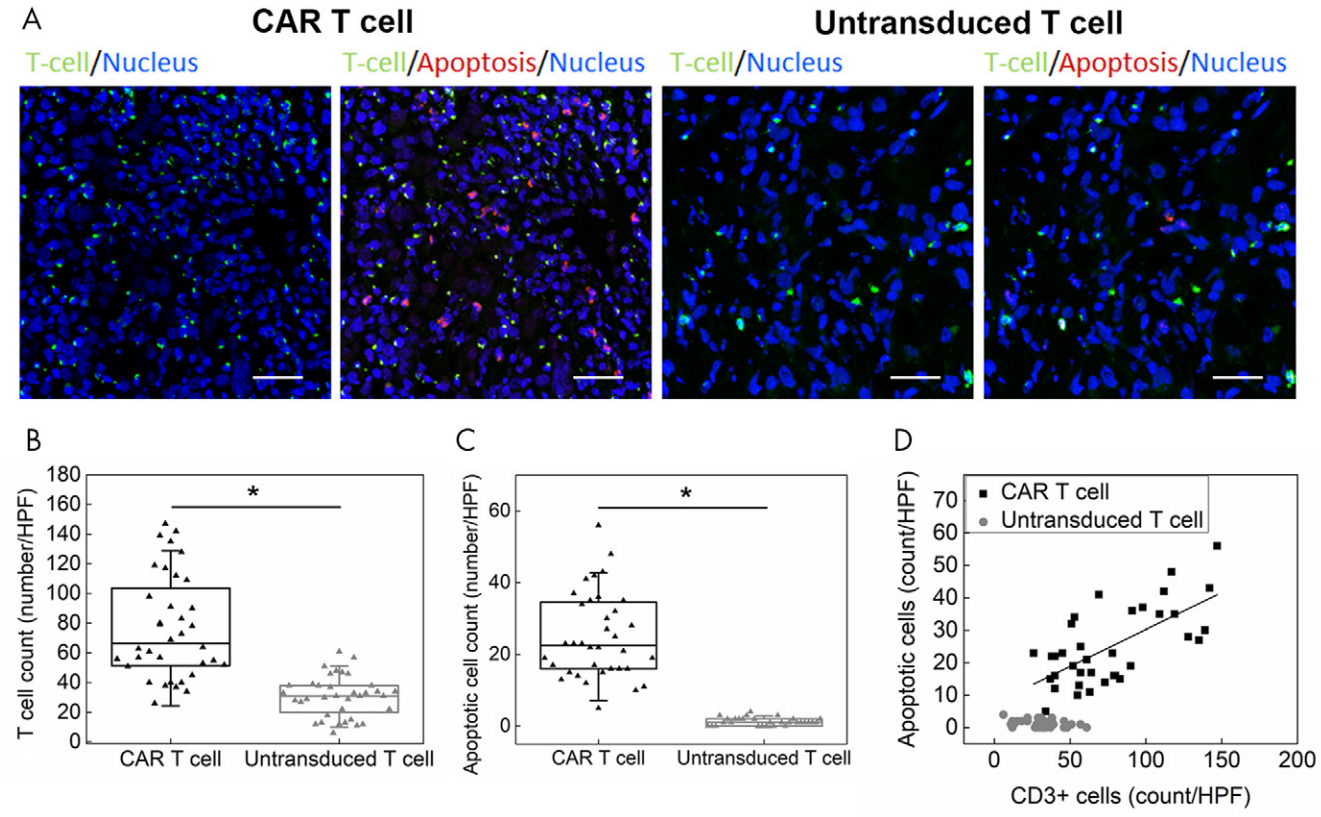

Figure 6: Histologic correlation of T-cell infiltration and cell death. *A*, Confocal microscopy at 60× magnification of tumor tissues shows prominent chimeric antigen receptor (CAR) T-cell infiltrates (green) at day 2 after intravenous infusion in the proximity of apoptotic cells (red), as evidenced by positive transferase dUTP nick end labeling stain. Untransduced T-cell–treated tumor exhibits sparser T cells and apoptotic signals. Scale bar = 50 μm. *B*, High-power field (HPF) quantitation of T-cell numbers displays twice as many CAR T cells per HPF on average compared with untransduced T cells (**P* < .001). *C*, Apoptotic cell count in 72 HPFs shows higher numbers in CAR T-cell–treated tumors compared with controls (**P* < .001). *D*, The number of CAR T cells correlate to the number of apoptotic cells per field (Pearson *r* = 0.67), whereas untransduced T cells do not (Pearson *r* = −0.31).

oxygenation and not cell-specific intracellular partial pressure. Moreover, poorly vascularized tumors may not show a blood oxygen level–dependent effect. Our view is that cell-targeted PFC and ^{19}F MR oximetry is an important advance, as it eliminates tissue injury and measurement errors, and it yields absolute Po_2 (in millimeters of mercury) in a defined cell population.

Intracellular tumor Po_2 sensing using ^{19}F is only applicable to preclinical models in its current form, but Po_2 monitoring of PFC-labeled cell therapy products (18) is potentially translatable. These same methods could be extended to other cell types of therapeutic interest, such as natural killer, dendritic, and stem-progenitor cells. Moreover, reliable detection of potential Po_2 changes is ultimately limited by the obtainable ^{19}F signal-to-noise ratio of the labeled cells; thus, measurement reliability may suffer at lower clinical magnetic field strengths compared with the high field strength (11.7 T) used in the present study.

Overall, we show that ^{19}F MRI enables temporal measurements of tumor cell oxygen tension in response to CAR T-cell therapy. These data support the view that ^{19}F Po_2 MRI can provide insights into the modes of action of engineered T-cell immunotherapy against cancer. Ongoing efforts aim to understand the cellular basis of the delayed, transient hyperoxia measured in tumor cells with adoptive cell transfer, an observation that deviates from the sustained hyperoxic state seen with conventional chemotherapy delivery (15); these insights may help to improve the design of future engineered T cells and to inform the course of administered immunotherapy.

Author contributions: Guarantors of integrity of entire study, F.C., E.T.A.; study concepts/study design or data acquisition or data analysis/interpretation, all authors; manuscript drafting or manuscript revision for important intellectual content, all authors; approval of final version of submitted manuscript, all authors; agrees to ensure any questions related to the work are appropriately resolved, all authors; literature research, F.C., E.T.A.; experimental studies, F.C., B.I.L., D.L.; statistical analysis, F.C., R.C., K.M.; and manuscript editing, F.C., B.I.L., R.C., H.O., E.T.A.

Disclosures of Conflicts of Interest: F.C. Activities related to the present article: This study was funded through National Institutes of Health grants R01-EB017271, R01-EB024015 and R01-CA139579 and the California Institute for Regenerative Medicine grant LA1-C12-06919. Activities not related to the present article: disclosed no relevant relationships. Other relationships: disclosed no relevant relationships. **B.I.L.** Activities related to the present article: This study was funded through National Institutes of Health grants R01-EB017271, R01-EB024015 and R01-CA139579 and the California Institute for Regenerative Medicine grant LA1-C12-06919. Activities not related to the present article: author formerly employed by Scripps Research Institute. Other relationships: disclosed no relevant relationships. **R.C.** disclosed no relevant relationships. **D.L.** disclosed no relevant relationships. **K.M.** disclosed no relevant relationships. **H.O.** Activities related to the present article: disclosed no relevant relationships. Activities not related to the present article: author paid royalties fees for licensed IP as one of the inventors of the EGFRviii-CAR that has been exclusively licensed to Novartis. However, this did not influence the interpretation of the data sets in this manuscript at all because this author did not participate in the data interpretation part. Other relationships: patent US 62/653,901 Inventors: Hideho Okada et al. US 62/653,901 Trans-Antigen Targeting in Heterogeneous Cancers and Methods of Use Thereof US 62/653,929 Methods of Treating Glioblastomas US 62/654,012 Methods of Treating EGFR-vIII-Expressing Glioblastomas; exclusively licensed to Novartis Pharma and royal-

ties from Novartis Pharma. **E.T.A.** Activities related to the present article: disclosed no relevant relationships. Activities not related to the present article: disclosed no relevant relationships. Other relationships: founder and shareholder of Celsense.

References

1. Teicher BA. A systems approach to cancer therapy. (Antioncogenics + standard cytotoxics-->mechanism(s) of interaction). Cancer Metastasis Rev 1996;15(2):247–272.
2. Jain RK. Normalization of tumor vasculature: an emerging concept in antiangiogenic therapy. Science 2005;307(5706):58–62.
3. Newick K, O'Brien S, Moon E, Albelda SM. CAR T cell therapy for solid tumors. Annu Rev Med 2017;68(1):139–152.
4. Maus MV, June CH. Making better chimeric antigen receptors for adoptive T-cell therapy. Clin Cancer Res 2016;22(8):1875–1884.
5. Adusumilli PS, Cherkassky L, Villena-Vargas J, et al. Regional delivery of mesothelin-targeted CAR T cell therapy generates potent and long-lasting CD4-dependent tumor immunity. Sci Transl Med 2014;6(261):261ra151.
6. Tatum JL, Kelloff GJ, Gillies RJ, et al. Hypoxia: importance in tumor biology, noninvasive measurement by imaging, and value of its measurement in the management of cancer therapy. Int J Radiat Biol 2006;82(10):699–757.
7. Riess JG. Understanding the fundamentals of perfluorocarbons and perfluorocarbon emulsions relevant to in vivo oxygen delivery. Artif Cells Blood Substit Immobil Biotechnol 2005;33(1):47–63.
8. Garrelts JC. Fluosol: an oxygen-delivery fluid for use in percutaneous transluminal coronary angioplasty. DICP 1990;24(11):1105–1112.
9. Riess JG. Oxygen carriers ("blood substitutes")--raison d'etre, chemistry, and some physiology. Chem Rev 2001;101(9):2797–2920.
10. Delpuech JJ, Hamza MA, Serratrice G, Stébé MJ. Fluorocarbons as oxygen carriers. I. An NMR study of oxygen solutions in hexafluorobenzene. J Chem Phys 1979;70(6):2680–2687.
11. LoNostro P, Choi SM, Ku CY, Chen SH. Fluorinated microemulsions: A study of the phase behavior and structure. J Phys Chem B 1999;103(25):5347–5352.
12. Delpuech JJ, Hamza MA, Serratrice G. Determination of oxygen by a nuclear magnetic-resonance method. J Magn Reson 1979;36(2):173–179.
13. Mason RP, Shukla H, Antich PP. In vivo oxygen tension and temperature: simultaneous determination using 19F NMR spectroscopy of perfluorocarbon. Magn Reson Med 1993;29(3):296–302.
14. Sotak CH, Hees PS, Huang H-N, Hung M-H, Krespan CG, Raynolds S. A new perfluorocarbon for use in fluorine-19 magnetic resonance imaging and spectroscopy. Magn Reson Med 1993;29(2):188–195.
15. Kadayakkara DK, Janjic JM, Pusateri LK, Young WB, Ahrens ET. In vivo observation of intracellular oximetry in perfluorocarbon-labeled glioma cells and chemotherapeutic response in the CNS using fluorine-19 MRI. Magn Reson Med 2010;64(5):1252–1259.
16. Zhong J, Sakaki M, Okada H, Ahrens ET. In vivo intracellular oxygen dynamics in murine brain glioma and immunotherapeutic response of cytotoxic T cells observed by fluorine-19 magnetic resonance imaging. PLoS One 2013;8(5):e59479.
17. Ahrens ET, Flores R, Xu H, Morel PA. In vivo imaging platform for tracking immunotherapeutic cells. Nat Biotechnol 2005;23(8):983–987.
18. Ahrens ET, Helfer BM, O'Hanlon CF, Schirda C. Clinical cell therapy imaging using a perfluorocarbon tracer and fluorine-19 MRI. Magn Reson Med 2014;72(6):1696–1701.
19. Rose LC, Kadayakkara DK, Wang G, et al. Fluorine-19 Labeling of Stromal Vascular Fraction Cells for Clinical Imaging Applications. Stem Cells Transl Med 2015;4(12):1472–1481.
20. Janjic JM, Ahrens ET. Fluorine-containing nanoemulsions for MRI cell tracking. Wiley Interdiscip Rev Nanomed Nanobiotechnol 2009;1(5):492–501.
21. Hingorani DV, Chapelin F, Stares E, Adams SR, Okada H, Ahrens ET. Cell penetrating peptide functionalized perfluorocarbon nanoemulsions for targeted cell labeling and enhanced fluorine-19 MRI detection. Magn Reson Med 2020;83(3):974–987.
22. Chapelin F, Gao S, Okada H, Weber TG, Messer K, Ahrens ET. Fluorine-19 nuclear magnetic resonance of chimeric antigen receptor T cell biodistribution in murine cancer model. Sci Rep 2017;7(1):17748.
23. Ohno M, Ohkuri T, Kosaka A, et al. Expression of miR-17-92 enhances anti-tumor activity of T-cells transduced with the anti-EGFRvIII chimeric antigen receptor in mice bearing human GBM xenografts. J Immunother Cancer 2013;1:21.
24. Srinivas M, Morel PA, Ernst LA, Laidlaw DH, Ahrens ET. Fluorine-19 MRI for visualization and quantification of cell migration in a diabetes model. Magn Reson Med 2007;58(4):725–734.
25. Helfer BM, Balducci A, Nelson AD, et al. Functional assessment of human dendritic cells labeled for in vivo (19)F magnetic resonance imaging cell tracking. Cytotherapy 2010;12(2):238–250.
26. Constantinides C, Maguire ML, Stork L, et al. Temporal accumulation and localization of isoflurane in the C57BL/6 mouse and assessment of its potential contamination in 19 F MRI with perfluoro-crown-ether-labeled cardiac progenitor cells at 9.4 Tesla. J Magn Reson Imaging 2017;45(6):1659–1667.
27. Patrick MJ, Janjic JM, Teng H, et al. Intracellular pH measurements using perfluorocarbon nanoemulsions. J Am Chem Soc 2013;135(49):18445–18457.
28. Janjic JM, Srinivas M, Kadayakkara DK, Ahrens ET. Self-delivering nanoemulsions for dual fluorine-19 MRI and fluorescence detection. J Am Chem Soc 2008;130(9):2832–2841.
29. Fesnak AD, June CH, Levine BL. Engineered T cells: the promise and challenges of cancer immunotherapy. Nat Rev Cancer 2016;16(9):566–581.
30. Irving M, Vuillefroy de Silly R, Scholten K, Dilek N, Coukos G. Engineering chimeric antigen receptor T-cells for racing in solid tumors: don't forget the fuel. Front Immunol 2017;8:267.
31. Kawalekar OU, O'Connor RS, Fraietta JA, et al. Distinct Signaling of Coreceptors Regulates Specific Metabolism Pathways and Impacts Memory Development in CAR T Cells [Published correction appears in Immunity 2016;44(3):712.] Immunity 2016;44(2):380–390.
32. Benmebarek MR, Karches CH, Cadilha BL, Lesch S, Endres S, Kobold S. Killing mechanisms of chimeric antigen receptor (CAR) T cells. Int J Mol Sci 2019;20(6):E1283.
33. Ly JD, Grubb DR, Lawen A. The mitochondrial membrane potential (deltapsi(m)) in apoptosis; an update. Apoptosis 2003;8(2):115–128.
34. Kim R. Recent advances in understanding the cell death pathways activated by anticancer therapy. Cancer 2005;103(8):1551–1560.
35. Fishman JE, Joseph PM, Floyd TF, Mukherji B, Sloviter HA. Oxygen-sensitive 19F NMR imaging of the vascular system in vivo. Magn Reson Imaging 1987;5(4):279–285.
36. Duong TQ, Iadecola C, Kim SG. Effect of hyperoxia, hypercapnia, and hypoxia on cerebral interstitial oxygen tension and cerebral blood flow. Magn Reson Med 2001;45(1):61–70.
37. Duong TQ, Kim SG. In vivo MR measurements of regional arterial and venous blood volume fractions in intact rat brain. Magn Reson Med 2000;43(3):393–402.
38. Dardzinski BJ, Sotak CH. Rapid tissue oxygen tension mapping using 19F inversion-recovery echo-planar imaging of perfluoro-15-crown-5-ether. Magn Reson Med 1994;32(1):88–97.
39. Hees PS, Sotak CH. Assessment of changes in murine tumor oxygenation in response to nicotinamide using 19F NMR relaxometry of a perfluorocarbon emulsion. Magn Reson Med 1993;29(3):303–310.
40. van der Sanden BP, Heerschap A, Simonetti AW, et al. Characterization and validation of noninvasive oxygen tension measurements in human glioma xenografts by 19F-MR relaxometry. Int J Radiat Oncol Biol Phys 1999;44(3):649–658.
41. Shukla HP, Mason RP, Bansal N, Antich PP. Regional myocardial oxygen tension: 19F MRI of sequestered perfluorocarbon. Magn Reson Med 1996;35(6):827–833.
42. Braun RD, Lanzen JL, Snyder SA, Dewhirst MW. Comparison of tumor and normal tissue oxygen tension measurements using OxyLite or microelectrodes in rodents. Am J Physiol Heart Circ Physiol 2001;280(6):H2533–H2544.
43. Seddon BM, Honess DJ, Vojnovic B, Tozer GM, Workman P. Measurement of tumor oxygenation: in vivo comparison of a luminescence fiber-optic sensor and a polarographic electrode in the p22 tumor. Radiat Res 2001;155(6):837–846.
44. Ogawa S, Lee TM, Kay AR, Tank DW. Brain magnetic resonance imaging with contrast dependent on blood oxygenation. Proc Natl Acad Sci U S A 1990;87(24):9868–9872.